Probing the dynamical properties of the metastable bcc Fe_xCo_{1-x} phase

B. Laenens,[1,2,*] N. Planckaert,[1] M. Sternik,[3] P. T. Jochym,[3] K. Parliński,[3] A. Vantomme,[1] and J. Meersschaut[1,2]
[1]*Instituut voor Kern- en Stralingsfysica and INPAC, K. U. Leuven, Celestijnenlaan 200 D, B-3001 Leuven, Belgium*
[2]*IMEC, Kapeldreef 75, B-3001 Leuven, Belgium*
[3]*Institute of Nuclear Physics, Polish Academy of Sciences, Radzikowskiego 152, 31-342 Kraków, Poland*
(Received 1 July 2008; revised manuscript received 25 May 2009; published 19 June 2009)

The stabilization of the metastable bcc-$Fe_xCo_{1-x}(0 \leq x \leq 0.25)$ phase is studied via the dynamical properties of the atoms. By means of nuclear resonant inelastic scattering of synchrotron radiation the phonon density of states (PDOS) spectra of Fe in bcc and fcc Fe_xCo_{1-x} are obtained. We analyze the measured PDOS spectra using first-principles calculations of phonon vibrations. Theoretical models of the thermodynamic unstable bcc phase, the stable fcc phase, as well as the bcc-Fe_4/Co_4 superlattice are constructed. Via calculations of the force constants and the phonon-dispersion relations we show that the bcc-Fe_xCo_{1-x} phase confined between two adjacent bcc-Fe layers can be stabilized by the Fe atoms in the Fe_xCo_{1-x} layer.

DOI: 10.1103/PhysRevB.79.224303 PACS number(s): 63.20.−e, 64.60.My, 76.80.+y

I. INTRODUCTION

The development of advanced deposition techniques opened the possibility to study the physical properties of thermodynamically unstable phases. The formation of these metastable phases can be induced by epitaxial growth. The knowledge of the interatomic forces and thus the dynamical vibrations in thermodynamical and nonthermodynamical phases would contribute to the understanding of the stabilization process. The present paper focuses on the atomic vibrations in the metastable bcc-$Fe_{0.1}Co_{0.9}$ phase and the stable fcc-$Fe_{0.1}Co_{0.9}$ phase using an experimental as well as an *ab initio* approach.

The phase diagram of pure Co exhibits two crystal structures. At low temperature Co crystallizes in the hcp phase while at temperatures above 704 K it undergoes a phase transition to the fcc phase. For Fe_xCo_{1-x} bulk alloys with $0.25 < x \leq 1$ the thermodynamically stable bcc crystal phase is observed.[1] For $0 \leq x \leq 0.25$ a mixed phase of bcc and fcc is reported. However techniques such as molecular beam epitaxy (MBE) make it possible to obtain the metastable bcc-Fe_xCo_{1-x} phase[2–4] for $0 \leq x \leq 0.25$. For example, it has been demonstrated that it is possible to stabilize $Fe_xCo_{1-x}(0 \leq x \leq 0.25)$ in the bcc phase via epitaxial growth in ZnSe/GaAs.[4] Alternatively, pure Co can be stabilized in the bcc phase in Fe/Co superlattices grown on MgO(100) up to a critical Co thickness of 2.1 nm.[5] Generally thicker Co layers are found to adopt the fcc phase. In this work both mechanisms are used to obtain the metastable bcc phase. That is, $[Fe/Fe_xCo_{1-x}]_{20}(x=0.1,0.2)$ multilayers are epitaxially grown to study the influence of the adjacent Fe layers and the Fe impurities on the stabilization process of the bcc-Co phase.

The dynamical properties are embodied in the phonon density of states (PDOS), from which one can deduce the thermodynamic properties such as the free energy, the entropy, or the vibrational amplitude. In nanostructures, including these ultrathin films, it is difficult to probe the PDOS by established methods such as neutron inelastic scattering. On the other hand, the recently developed technique of nuclear resonant inelastic scattering (NIS) makes it possible to probe the site-selective PDOS of nanostructures due to the high brilliance of undulator-based synchrotron facilities and its sensitivity to probe nuclei (e.g., ^{57}Fe).[6,7] Recent publications illustrate the various possibilities of NIS to probe the partial PDOS of dilute Fe atoms in alloys[8] and of nanosize precipitates, clusters,[9] multilayers, and thin films.[10–15] For bcc-Co nanostructures, nuclear probes have been successfully used to study structural and magnetic properties of the metastable phase.[16,17] Here, we use the ^{57}Fe isotope to study the atomic vibrations via NIS in metastable bcc-Fe_xCo_{1-x} and stable fcc-Fe_xCo_{1-x} thin films.

Recently the dynamical properties of crystals and low-periodicity multilayers are successfully studied using first-principles calculations. For example, the phonon-dispersion relations in the bcc-Fe crystal are very well reproduced within the spin-polarized general gradient approximation (GGA) technique.[18,19] These methods are also applied to analyze the stability of Fe/Au multilayers.[20] The first-principles methods give opportunity to determine the magnetic properties of calculated systems. The magnetic moments distribution and the magnetic anisotropy energy of Fe/Co superlattices have been already reported in Ref. 21. The fixed spin moment *ab initio* calculations have been used to study the effect of magnetism on the mechanical stability of bcc-Fe and bcc-Co.[22]

The accuracy of modern quantum-mechanical methods for describing condensed matter from first principles allows us to theoretically model the bcc-Fe_xCo_{1-x} and fcc-Fe_xCo_{1-x} phases in a bulk configuration and a Fe/Co multilayer composition.

II. SAMPLE PREPARATION AND EXPERIMENTS

We combined multilayered growth, as described in Ref. 23, with the procedure of Prinz,[2] i.e., the addition of Fe atoms to the Co layer, to obtain the bcc-Co phase. Samples of bcc-Co doped with 10 and 20at. % ^{57}Fe are grown with MBE. The samples are composed of a Au (100 nm) buffer layer grown at 180 °C on a ^{56}Fe(6 nm) precovered MgO(100) substrate. Prior to the deposition of the Fe_xCo_{1-x} layer the buffer layer was annealed at 600 °C for 30 min.

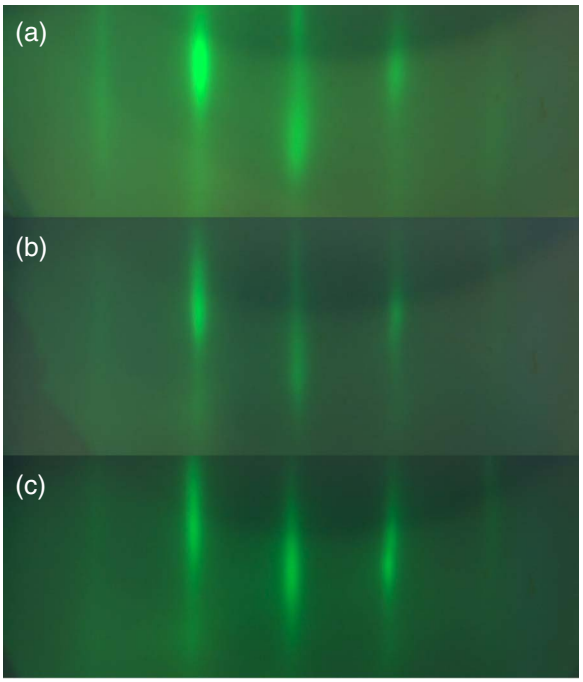

FIG. 1. (Color online) RHEED patterns observed during the growth in the Fe/bcc-Co multilayer on MgO(100) for (a) the first Fe layer on the Au buffer layer, (b) the fourth Co layer, and (c) the thirteenth Co layer.

The Fe_xCo_{1-x} layer is codeposited with isotopically enriched $^{57}Fe(95\%)$ whereas the iron constituting the buffer layers consists of the nonresonant ^{56}Fe isotope. Taking into account the difference in atomic density and the $^{57}Fe_{0.1}Co_{0.9}$ atomic ratio the deposition rates for ^{57}Fe and Co were 0.010 and 0.085 Å/s, respectively. To increase the total amount of ^{57}Fe in the samples to the level required for NIS the FeCo layer is repeated 20 times and stabilized with ^{56}Fe layers in between, similar as described in Refs. 3, 5, and 23. The $[^{56}Fe(2.4\ nm)/^{57}Fe_{0.1}Co_{0.9}(1.7\ nm)]_{20}$ multilayers are capped with 2 nm of Au deposited at room temperature. Apart from the beneficial effects of the Au base and capping layer to improve the epitaxial growth[24] and to prevent the oxidation, respectively, the deposition of the Fe/Fe_xCo_{1-x} multilayer between the denser Au layers leads to a significant x-ray intensity enhancement within the enriched Co region. This phenomenon, known as the waveguide effect, has been used before in nuclear-scattering experiments to increase the count rate of the delayed photons.[25]

The characterizations of the bcc-Fe_xCo_{1-x} samples by means of reflection high-energy electron diffraction (RHEED) and high angle x-ray diffraction (XRD) indicate the existence of the bcc phase and epitaxial growth in the multilayer. The RHEED patterns in Fig. 1 of the two Co layers recorded at different stages of deposition (panels b and c) are seen to have the same symmetry as bcc Fe (panel a). Figure 2(a) displays the high angle x-ray diffraction scan of the bcc-$Fe_{0.1}Co_{0.9}$ multilayer obtained with an x-ray diffractometer and a Cu x-ray source $[K_\alpha(Cu)=1.5401\ Å]$. The scan shows a diffraction peak around 44° resulting from the fcc (200) reflection of the Au buffer layer. The satellite peaks result from the Fe/FeCo superstructure as reported

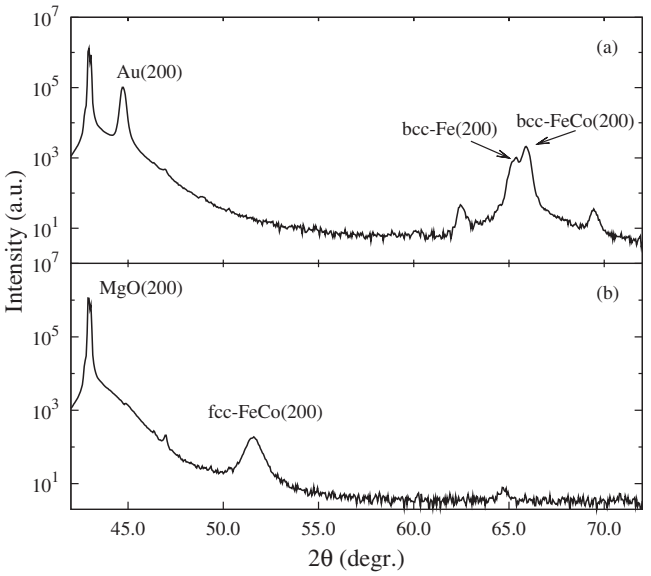

FIG. 2. High-angle x-ray diffractometry scans (θ-2θ) of (a) the bcc-Co sample $[^{56}Fe(2.4\ nm)/^{56}Fe_{0.1}Co_{0.9}(1.7\ nm)]_{20}$ and (b) the reference fcc-Co sample $^{57}Fe_{0.1}Co_{0.9}(50\ nm)$.

by Dekoster *et al.*[5] A confirmation of the presence of the bcc structure is given by the double diffraction peak around 65°. The peaks are attributed to the bcc-Fe(200) and the bcc-$Fe_{0.1}Co_{0.9}(200)$ reflections. From this bcc-$Fe_{0.1}Co_{0.9}(200)$ diffraction peak a lattice parameter of 2.83 Å is derived, which is close to the lattice parameter of 2.84 Å reported for a bcc-$Fe_{0.11}Co_{0.89}$ film grown on MgO(100).[26]

To compare the PDOS of the metastable bcc-FeCo with a reference PDOS, an fcc-$Fe_{0.1}Co_{0.9}$ sample is grown with a thickness larger than the critical bcc-Co thickness limit of 2.1 nm. The reference sample consists of a single $^{57}Fe_{0.1}Co_{0.9}$ film of 50 nm thickness deposited at 150 °C directly on an MgO(100) substrate and a 2-nm-thick Au capping layer. Figure 2(b) shows the diffraction spectrum of the fcc-$Fe_{0.1}Co_{0.9}$ reference sample with the fcc-$Fe_{0.1}Co_{0.9}(200)$ diffraction peak[27] located at 52°. From this peak a lattice parameter of 3.54 Å is calculated.

The dynamics of the bcc-$Fe_xCo_{1-x}(x=0.1,0.2)$ and the fcc-$Fe_{0.1}Co_{0.9}$ samples were studied via nuclear resonant inelastic scattering of synchrotron radiation at beamline ID18 of the ESRF.[28] The radiation was monochromatized to a bandwidth of 2 meV with a high-resolution monochromator. The delayed fluorescence photons were measured by an avalanche photodiode placed close to the sample to cover the largest possible solid angle. An energy range of ±70 meV was scanned in steps of 0.5 meV. All data were taken at room temperature with collection times of ~5–10 h per spectrum. The local vibrational densities of states of ^{57}Fe in bcc-Co and fcc-Co were extracted from the measured excitation probabilities after subtracting the elastic peak contribution by using the procedure described in Ref. 29.

III. COMPUTATIONAL PROCEDURE

Spin-polarized density-functional total-energy calculations are performed within the GGA method using the VASP

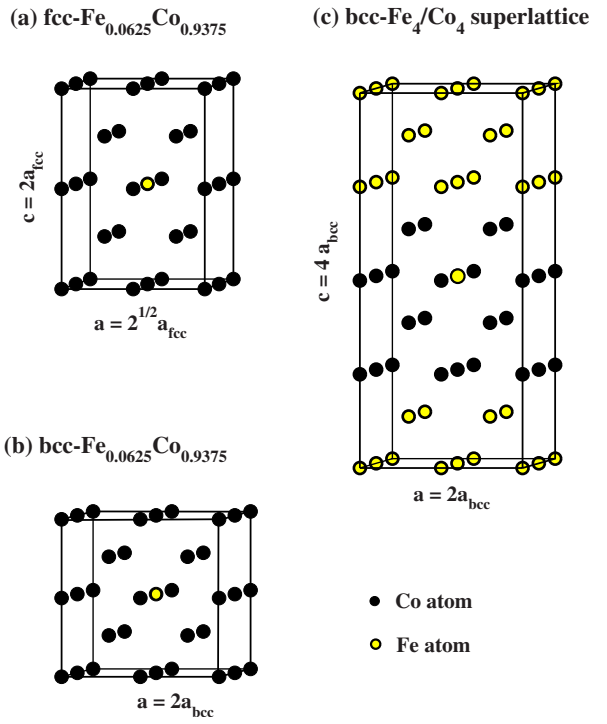

FIG. 3. (Color online) The supercell of the (a) bulk fcc $Fe_{0.0625}Co_{0.9375}$, (b) bulk bcc $Fe_{0.0625}Co_{0.9375}$, and (c) bcc-Fe_4/Co_4 superlattice.

package.[30,31] The valence electrons for each atom (electron configuration: d^8s^1 and d^7s^1 for the Co and Fe atoms, respectively) are represented by plane-wave expansions with an energy cutoff of 350 eV. The wave functions in the core region are evaluated using the full potential projector augmented-wave method.[32] The integrations in the reciprocal space are performed on a $4\times4\times4$ grid using the Monkhorst-Pack scheme. During the optimization the Hellmann-Feymann (H-F) forces and the stress tensor are calculated. The crystal structure optimization is finished when residual forces were less than 10^{-5} eV/Å and stresses are less than 0.1 kbar.

We started the *ab initio* calculations with the optimization of the bulk fcc-Co and bcc-Co crystals represented by the $Fm3m$ and $Im3m$ symmetry space groups, respectively. The obtained lattice parameters are $a_{fcc}=3.50$ Å and $a_{bcc}=2.80$ Å for the fcc-Co and bcc-Co crystals, respectively. These results are in good agreement with the experimental values of 3.55 and 2.83 Å deduced from the XRD spectra. The deviation of 1.5% from the experimental lattice constants is typical for density-functional theory calculations. The ground-state energy obtained for the fcc structure is 144 meV/atom lower than the calculated value for the bcc structure which agrees with the fact that the fcc structure is energetically more favorable than the bcc structure.

Next, in the relevant supercell consisting of 16 cobalt atoms one cobalt atom was replaced by one iron atom as illustrated in Fig. 3. All calculations are performed under the periodic boundary conditions. Therefore structures (a) and (b) are, respectively, the ideal fcc and bcc crystals based on Co atoms with Fe impurities placed periodically in a fixed site of the unit cell. These crystals are further called fcc-$Fe_{0.0625}Co_{0.9375}$ and bcc-$Fe_{0.0625}Co_{0.9375}$ though their actual symmetries are $P4/mmm$ and $Pm3m$, respectively. The calculated lattice parameters for the tetragonal $P4/mmm$ structure are $a=\sqrt{2}a_{fcc}=4.95$ Å and $c=2a_{fcc}=7.00$ Å and the lattice constant for the cubic $Pm3m$ structure is $a=2a_{bcc}=5.60$ Å. The difference of 66 meV/atom between the ground-state energies of the doped bcc-Co and fcc-Co crystals is two times smaller than the calculated values of 144 eV/atom for the pure Co crystals.

So far we performed calculations on the bulk fcc and bcc crystals. However to represent the experimentally investigated $^{56}Fe(2.4\ nm)/[^{57}Fe_{0.1}Co_{0.9}(1.7\ nm)]_{20}$ thin film by a theoretical model a bcc-Fe_4/Co_4 superlattice [Fig. 3(c)] is considered as a model structure of the measured multilayer. The number of repetitions and the thickness of the layers in the model are limited to reduce the calculation time. In this structure we replaced a Co atom of the middle monolayer with an Fe atom. The Fe concentration x in the Co layer is 0.0625, which is the same concentration as used in the bulk sample discussed above. The calculated lattice constants are $a=5.62$ Å and $c=11.33$ Å.

Next, for the optimized structures the phonon-dispersion relations are calculated using the direct method.[33,34] The dynamical matrix of the crystal is constructed from the H-F forces generated while displacing atoms from their equilibrium positions. The number of required displacements is determined by the symmetry of the crystal and by the number of nonequivalent atoms. For a pure bcc-Co and fcc-Co crystal only one displacement is sufficient but for a bcc-Fe_4/Co_4 superlattice, shown in Fig. 3(c), a complete set of Hellmann-Feynman forces is obtained from 32 independent atomic displacements. The amplitude of the displacements equals 0.03 Å. To minimize systematic errors we applied displacements in positive and negative directions. Finally the phonon frequencies are obtained by the diagonalization of the dynamical matrix for each wave vector. The Bravais symmetry group of the crystal indicates the high-symmetry points and the directions in the reciprocal lattice for which the phonon-dispersion relations are presented. The direct method gives the exact phonon frequencies at the wave vectors commensurate with the size of the supercell and independent on the range of the interaction. Moreover all phonon branches are well reproduced when the magnitude of the force constants decreases relatively fast. All structures considered in this work satisfy this condition.

IV. RESULTS AND DISCUSSION

In this section we compare the experimental results with first-principles calculations and discuss the effect of the adjacent Fe layers and Fe impurities on the stabilization of the metastable bcc-Co phase in the multilayer structure. We start with the comparison between the calculated phonon-dispersion relations and PDOS of the pure and the doped crystals and superlattices.

In Fig. 4 the phonon-dispersion relations and phonon density of states spectra calculated for the pure fcc-Co, bcc-Co crystals, and the bcc-Fe_4/Co_4 superlattice are presented. In

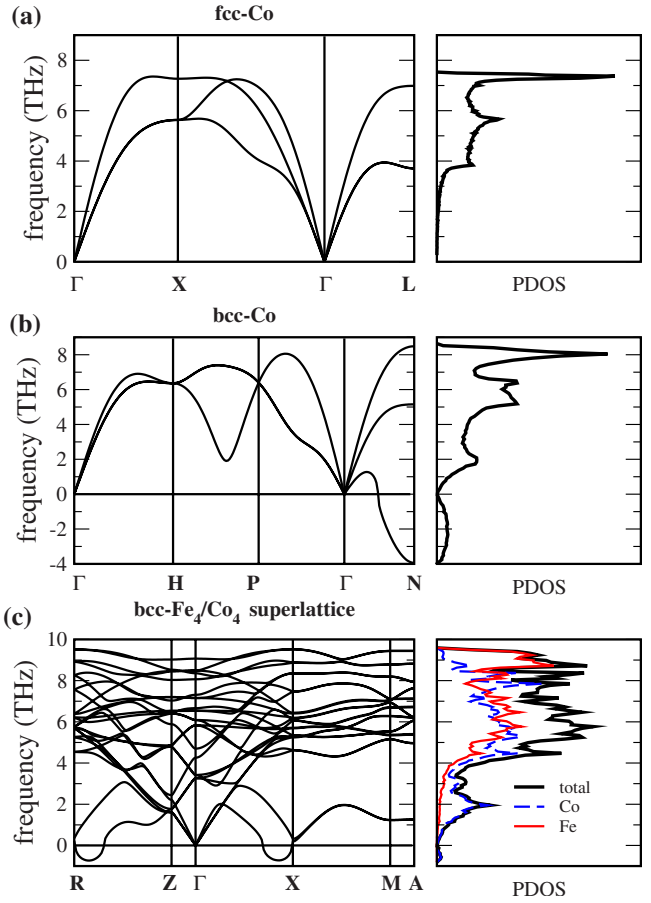

FIG. 4. (Color online) (left) The phonon-dispersion relations and (right) the PDOS calculated for (a) fcc-Co crystal, (b) bcc-Co crystal, and (c) bcc-Fe_4/Co_4 superlattice.

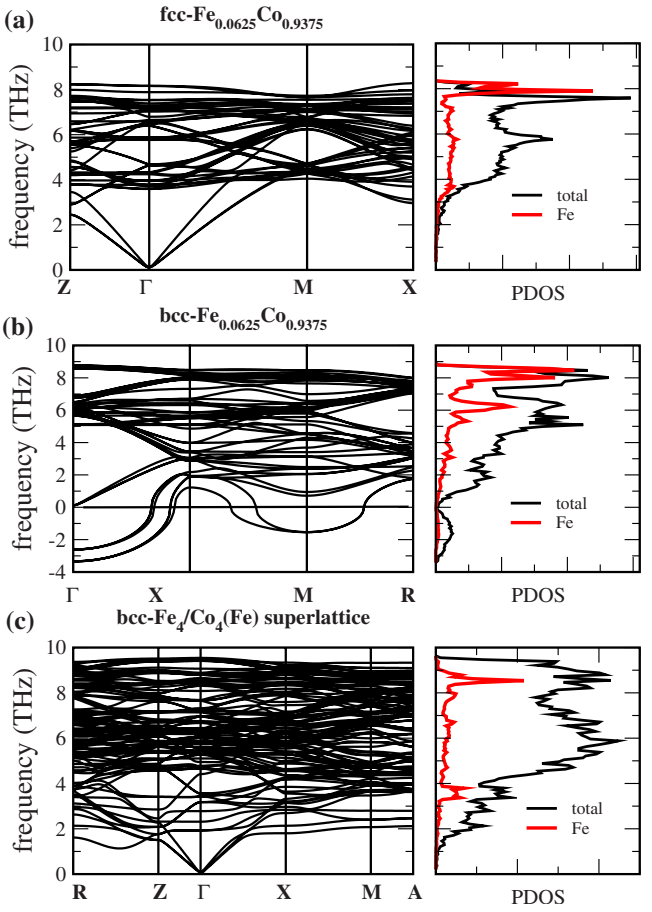

FIG. 5. (Color online) (left) The phonon-dispersion relations and (right) the total and partial (calculated for Fe probe atoms) PDOS calculated for (a) fcc-$Fe_{0.0625}Co_{0.9375}$ crystal, (b) bcc-$Fe_{0.0625}Co_{0.9375}$ crystal, and (c) bcc-Fe_4/Co_4 superlattice. All structures are illustrated in Fig. 3. The partial PDOS spectra for Fe probe atoms are multiplied by a factor of 5.

case of the fcc structure [Fig. 4(a)] all frequencies are positive indicating that the fcc-Co phase is stable. However, for the bulk bcc structure [Fig. 4(b)] imaginary frequencies are observed at the exact point *N* (presented here as negative values). These imaginary frequencies, as reported in Ref. 22, indicate the instability of the bcc-Co crystal. Imaginary frequencies are also observed for bcc-Fe_4/Co_4 [Fig. 4(c)]. The phonon density of states spectra calculated for Co and Fe atoms, respectively [see the right panel of Fig. 4(c)], show that all frequencies related to the Fe vibrations are positive, in contrary to the Co vibrations. Hence, we can conclude that the bcc-Co layer between two stable bcc-Fe layers is unstable.

When one of the Co atoms in the Co crystals or the Fe/Co superlattice are replaced by an additional Fe atom the vibrational spectra change as it is shown in Fig. 5. The partial PDOS presented in the right panels of the figure only show the contribution of the Fe probe atoms to the total PDOS. For the bcc-$Fe_{0.0625}Co_{0.9375}$ and fcc-$Fe_{0.0625}Co_{0.9375}$ phases the vibrations of the Fe atoms mainly contribute into the high-frequency region of the spectrum [Figs. 5(a) and 5(b)]. The amount of Fe atoms introduced into the bcc-Co phase is insufficient to stabilize this phase [Fig. 5(b)]. The instability of this system is manifested by the appearance of the soft mode at the exact point Gamma. Imaginary frequencies are clearly present in the total PDOS of the bcc crystal while they are nearly absent in the partial Fe PDOS. Thus the instability of the bcc phase is related to the vibrations of the Co atoms.

Table I summarizes magnitudes of the independent parameters of the on-site force constants matrices of Co and Fe atoms in the various bcc and fcc crystals. The site symmetry of the cubic or lower symmetry structures causes that the interaction between impurity and host is described by one or several independent parameters. For the lower symmetry cases the interval of the parameters is given. We find that the calculated force constants of Fe atoms placed in the bcc-

TABLE I. Calculated on-site force constants of Fe and Co atoms in the various bcc and fcc crystals.

	Force constant (eV/Å)		
Co in bcc-Co	7.7	Co in fcc-Co	8.4
Fe in bcc-Fe	11.7	Fe in fcc-Fe	8.4
Fe in bcc-FeCo	10.3	Fe in fcc-FeCo	9.5–9.9
Co in bcc-FeCo	7.6–9.3	Co in fcc-FeCo	8.2–9.3

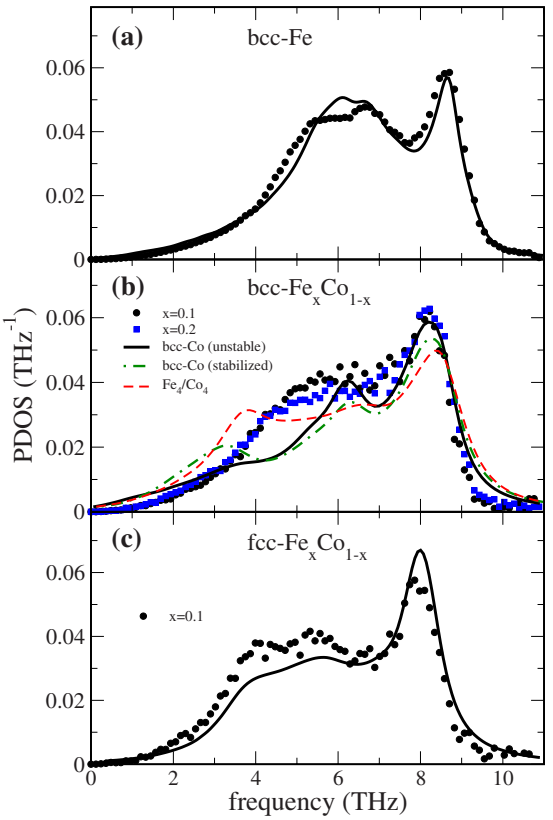

FIG. 6. (Color online) The measured and calculated PDOS of ^{57}Fe atoms in three different structures are compared: (a) the bcc-Fe crystal, (b) the bcc-Co structure doped by Fe atoms, and (c) the fcc-Co crystal doped by Fe atoms. In the calculations the ideal bulk systems (as described in the text) are used. The calculated spectra are convoluted with a Lorentzian function with a half width of 2 or 4 meV for the Fe crystal and Fe$_x$Co$_{1-x}$ crystals, respectively.

FeCo system are higher than the force constant of a Co atom in the bcc-FeCo crystal. Higher values of the force constants cause an increase in phonon frequencies. This is reflected in the PDOS spectra of Figs. 5(a) and 5(b); i.e., the main contribution to the partial PDOS is located at the high-frequency region. Moreover the high-frequency limit of the partial PDOS calculated for both bcc structures is larger than that obtained for the fcc-Co phase. Furthermore a noticeable increase in the force constants of Co atoms in the nearest neighborhood of an Fe impurity is also found. In bcc-Fe$_x$Co$_{1-x}$, their magnitudes rise from 7.6 to 9.3 eV/A for Co atoms occupying sites far away from or close to Fe atoms, respectively. At higher concentrations of Fe atoms this effect leads to the stabilization of the bcc-Fe$_x$Co$_{1-x}$ system. It follows that the Fe atoms incorporated in the bcc-Co system can stabilize their nearest neighborhood.

The calculations performed on the Fe$_4$/Co$_4$ superlattice with a doped Co layer reveal that the full stabilization of the bcc-Co phase is established when the bcc-Co structure doped by Fe atoms is placed between two bcc-Fe layers [Fig. 5(c)].

Now that a theoretical representation of the metastable bcc-Co phase is found, a comparison between the theoretical PDOS and the experimental results can be made. Figure 6 shows the experimental vibrational PDOS for ^{57}Fe in a bcc-Fe foil, and in the bcc-Fe$_x$Co$_{1-x}$ and fcc-Fe$_{0.1}$Co$_{0.9}$ thin films, respectively. The PDOS of the three systems have a similar shape. Yet a clear shift toward lower frequencies is observed for the PDOS of the bcc-Co with respect to the PDOS of bulk Fe, and the PDOS of the fcc-Co sample is shifted to even lower frequencies. To understand the origin of this behavior a comparison between the experimental and the calculated PDOS is necessary. The theoretical PDOS spectra of Fe probe atoms placed in the bcc-Co and fcc-Co crystals are obtained using the procedure described in Sec. III. The spectrum calculated for bulk Fe is taken from Ref. 19. To make a direct comparison between the experimental and the theoretical PDOS, the calculated PDOS is convoluted with a Lorentzian function with a half width of 2 and 4 meV for the pure bcc-Fe crystal and the Fe$_x$Co$_{1-x}$ systems, respectively. In the *ab initio* approach only single units of Co atoms can be replaced by Fe atoms. Therefore the calculations are performed for samples with a slightly lower iron concentration than the measured samples, that is Fe$_{0.0625}$Co$_{0.9375}$ for the calculated crystals compared to Fe$_{0.1}$Co$_{0.9}$ for the measured sample. However, for such small Fe impurities, a change in concentration has no big impact on the PDOS, as illustrated by the measured PDOS of bcc-Fe$_x$Co$_{1-x}$ with x=0.1 and 0.2 in Fig. 6(b).

The partial PDOS measured for ^{57}Fe atoms placed in the fcc-Co crystal compares well to the calculated spectra. The position and intensity of the high-frequency peak are reproduced very well whereas the intensities of the lower frequency peaks are slightly underestimated for fcc-FeCo. These discrepancies are attributed to the ideal crystal structure used in the calculations, in contrast to the measured sample with randomly distributed ^{57}Fe.

The experimental PDOS of bcc-FeCo in panel b of Fig. 6 is compared to three different theoretical PDOS. The solid line represents the calculated PDOS of the bcc-Fe$_{0.0625}$Co$_{0.9375}$ crystal. As discussed above, the bcc-Fe$_{0.0625}$Co$_{0.9375}$ structure displays anharmonic modes which make this crystal unstable. In the harmonic approximation these modes have an imaginary frequency. Anharmonic modes are not taken into account in the calculation of the phonon density of states [solid line in Fig. 6(b)]. Hence the low-frequency region cannot be correctly described. Yet the position of the high-frequency peak is well reproduced and agrees very well with the experimental one.

In the harmonic approximation the lattice dynamics is characterized by a collection of noninteracting harmonic oscillators. The imaginary modes, however, are described by an anharmonic oscillator vibrating in a double-well potential. Yet for sufficiently large amplitudes an imaginary mode vibrates near the harmonic region of the potential and its frequency turns to a real value (i.e., the system is stabilized).[35] These larger displacements can be generated by the thermal vibrations of the atoms. In our second theoretical model we calculate the phonon frequencies of the bulk bcc-Fe$_{0.0625}$Co$_{0.9375}$ crystal taking into account an additional set of H-F forces. The additional H-F forces originate from the frozen soft modes with sufficiently large amplitudes to stabilize the crystal. From the known eigenvectors of the phonon modes we find the displacement patterns related to the particular soft mode. The realistic displacement ampli-

tude of the frozen mode corresponding to room temperature is less than 0.25 Å. The room-temperature conditions are fulfilled assuming the amplitude of the soft modes $Q = 5$ Å $(\text{amu})^{1/2}$. Then the additional H-F forces imposed by the soft modes are computed and included in the construction of the dynamical matrix. The obtained phonon frequencies are all positive and considered in the phonon density of states represented by the dash-dotted line in Fig. 6(b). The presence of the low-frequency peak at 3 THz is the main difference between the calculated spectra mentioned so far. The position of the high-frequency peak stays almost unchanged. With this approach all frequencies are taken into account in the phonon density of states improving its behavior at lower frequencies.

The third dashed line represents the partial PDOS calculated for Fe probe atoms placed into the bcc-Co layer of the bcc-Fe_4/Co_4 superlattice. Although the structure is stable its thickness is not sufficient to exclude the interfacial interaction between the Fe probe atoms and Fe atoms placed in the bcc-Fe layers. This interaction leads to the increase in the force constants of Fe probe atoms and successively to the increase in its phonon frequencies. Comparing the discrete phonon spectra presented in panels b and c of Fig. 5 it is clearly seen that the large intensity peak at 8 THz observed in bulk bcc-$Fe_{0.0625}Co_{0.9375}$ almost vanishes in a thin bcc-Co layer. It results in a nonsymmetric shape of the high-frequency peak of the convoluted spectrum presented in Fig. 6(b). Taking into account the thickness of 1.7 nm of the bcc-Co layer in the measured sample, the influence of the interaction between the probe and Fe layer is negligible in the measurements. We therefore conclude that the high-frequency peak of the bulk bcc crystal seems to be more representative than the one computed for the Fe_4/Co_4 superlattice. The calculations on more complex and larger supercells with randomly distributed Fe impurities in the Co-layer would improve the agreement between experiment and calculations but they are at the moment computationally too demanding. Besides, the calculations do not take into account the strain present in the thin films. Such a strain is typically observed in epitaxially grown ultrathin films[36,37] and is found to influence the PDOS.[14,15]

V. CONCLUSIONS

The technique of nuclear resonant inelastic scattering allowed us to obtain the experimental PDOS of Fe in metastable bcc-Fe_xCo_{1-x} and stable fcc-Fe_xCo_{1-x} with $0 \leq x \leq 0.25$. The shift in the high-frequency peak observed in the experimental PDOS is very well reproduced in the calculations. The shift is generated by the differences in the magnitude of the interatomic forces of Fe atoms introduced in the various systems. These differences are probably caused by significant changes in the electronic charge distribution. Using *ab initio* calculations we have proven that the metastable bcc-Co layer between adjacent Fe layers can be stabilized by the addition of Fe atoms in the Co layer. The iron atoms included in the bcc-Co system cause the rise of force constant values in its nearest neighborhood and stabilize its surroundings in a bcc structure. Thus both the Fe layers and the Fe atoms diluted in the Co layer play a very important role in the stabilization process. Finally this work demonstrates the importance to study atomic vibrations and interatomic forces to investigate the phase stability conditions.

ACKNOWLEDGMENTS

We wish to thank A. Chumakov and the staff at the ESRF beamline ID18 cordially for their help during the experiment and M. Rennhofer, T. Ślezak, and M. Zajac. The work was supported by the European Community via Grant No. NMP4-CT-2003-001516 (DYNASYNC), by the FWO (Fund for Scientific Research Flanders), by the Interuniversity Attraction Pole (IUAP, Grant No. P6/42), by the Concerted Action of the K. U. Leuven (Grant No. GOA/2004/02), by the Centers of Excellence Programme (INPAC, Grant No. EF/05/005), and by COST Action 19, as well as by the Polish Government (MNiSW) under Contract No. 44/N-COST/2007/0.

*bart.laenens@fys.kuleuven.be

[1] T. Nishizawa and K. Ishida, Bull. Alloy Phase Diagrams **5**, 250 (1984).
[2] G. A. Prinz, Phys. Rev. Lett. **54**, 1051 (1985).
[3] Ph. Houdy, P. Boher, F. Giron, F. Pierre, C. Chappert, P. Beauvillain, K. Le Dang, P. Veillet, and E. Velu, J. Appl. Phys. **69**, 5667 (1991).
[4] C. J. Gutierrez, G. A. Prinz, J. J. Krebs, M. E. Filipkowski, V. G. Harris, and W. T. Elam, Z. Phys. B: Condens. Matter **126**, 232 (1993).
[5] J. Dekoster, E. Jedryka, C. Mény, and G. Langouche, Europhys. Lett. **22**, 433 (1993).
[6] M. Seto, Y. Yoda, S. Kikuta, X. W. Zhang, and M. Ando, Phys. Rev. Lett. **74**, 3828 (1995).
[7] W. Sturhahn, T. S. Toellner, E. E. Alp, X. Zhang, M. Ando, Y. Yoda, S. Kikuta, M. Seto, C. W. Kimball, and B. Dabrowski, Phys. Rev. Lett. **74**, 3832 (1995).
[8] M. Seto, Y. Kobayashi, S. Kitao, R. Haruki, T. Mitsui, Y. Yoda, S. Nasu, and S. Kikuta, Phys. Rev. B **61**, 11420 (2000).
[9] Y. Tsunoda, Y. Kurimoto, M. Seto, S. Kitao, and Y. Yoda, Phys. Rev. B **66**, 214304 (2002).
[10] R. Röhlsberger, W. Sturhahn, T. S. Toellner, K. W. Quast, P. Hession, M. Hu, J. Sutter, and E. E. Alp, J. Appl. Phys. **86**, 584 (1999).
[11] B. Handke, A. Kozlowski, K. Parlinski, J. Pzrzewoznik, T. Slezak, A. I. Chumakov, L. Niesen, Z. Kakol, and J. Korecki, Phys. Rev. B **71**, 144301 (2005).
[12] M. Walterfang, W. Keune, E. Schuster, A. T. Zayak, P. Entel, W. Sturhahn, T. S. Toellner, E. E. Alp, P. T. Jochym, and K. Parlinski, Phys. Rev. B **71**, 035309 (2005).
[13] J. Łażewski, J. Korecki, and K. Parlinski, Phys. Rev. B **75**, 054303 (2007).

[14] S. Stankov, R. Röhlsberger, T. Ślęzak, M. Sladecek, B. Sepioł, G. Vogl, A. I. Chumakov, R. Rüffer, N. Spiridis, J. Łażewski, K. Parlinski, and J. Korecki, Phys. Rev. Lett. **99**, 185501 (2007).
[15] T. Ślęzak, J. Łażewski, S. Stankov, K. Parlinski, R. Reitinger, M. Rennhofer, R. Rüffer, B. Sepiol, M. Ślęzak, N. Spiridis, M. Zająac, A. I. Chumakov, and J. Korecki, Phys. Rev. Lett. **99**, 066103 (2007).
[16] B. Swinnen, J. Dekoster, S. Cottenier, J. Meersschaut, S. Demuynck, G. Langouche, and M. Rots, Europhys. Lett. **37**, 621 (1997).
[17] L. Häggström, B. Kalska, E. Nordström, P. Blomqvist, and R. Wäppling, J. Alloys Compd. **347**, 252 (2002).
[18] A. Dal Corso and S. de Gironcoli, Phys. Rev. B **62**, 273 (2000).
[19] J. Łażewski, P. Piekarz, A. M. Oleś, and K. Parlinski, Phys. Rev. B **74**, 174304 (2006).
[20] M. Sternik, K. Parlinski, and J. Korecki, Phys. Rev. B **74**, 195405 (2006).
[21] A. Bergman, T. Burkert, B. Sanyal, S. Frota-Pessoa, L. Nordström, A. V. Ruban, S. I. Simak, and O. Eriksson, Phys. Rev. B **74**, 174409 (2006).
[22] H. C. Hsueh, J. Crain, G. Y. Guo, H. Y. Chen, C. C. Lee, K. P. Chang, and H. L. Shih, Phys. Rev. B **66**, 052420 (2002).
[23] J. P. Jay, E. Jedryka, M. Wojcik, J. Dekoster, G. Langouche, and P. Panissod, Z. Phys. B: Condens. Matter **101**, 329 (1996).
[24] N. Spiridis and J. Korecki, Appl. Surf. Sci. **141**, 313 (1999).
[25] R. Röhlsberger, H. Thomas, K. Schlage, E. Burkel, O. Leupold, and R. Rüffer, Phys. Rev. Lett. **89**, 237201 (2002).
[26] M. Wojcik, J. P. Jay, P. Panissod, E. Jedryka, J. Dekoster, and G. Langouche, Z. Phys. B: Condens. Matter **103**, 5 (1997).
[27] J. F. Calleja, Y. Huttel, M. C. Contreras, E. Navarro, B. Presa, R. Matarranz, and A. Cebollada, J. Appl. Phys. **100**, 053917 (2006).
[28] R. Rüffer and A. I. Chumakov, Hyperfine Interact. **97-98**, 589 (1996).
[29] V. G. Kohn and A. I. Chumakov, Hyperfine Interact. **125**, 205 (2000).
[30] G. Kresse and J. Hafner, Phys. Rev. B **47**, 558 (1993).
[31] G. Kresse and J. Furthmüller, Phys. Rev. B **54**, 11169 (1996); Comput. Mater. Sci. **6**, 15 (1996).
[32] P. E. Blöchl, Phys. Rev. B **50**, 17953 (1994); G. Kresse and D. Joubert, *ibid.* **59**, 1758 (1999).
[33] K. Parlinski, Z. Q. Li, and Y. Kawazoe, Phys. Rev. Lett. **78**, 4063 (1997).
[34] K. Parlinski, *Software* PHONON (Cracow, 2007).
[35] M. Sternik and K. Parlinski, J. Chem. Phys. **123**, 204708 (2005).
[36] S. Demuynck, J. Meersschaut, J. Dekoster, B. Swinnen, R. Moons, A. Vantomme, S. Cottenier, and M. Rots, Phys. Rev. Lett. **81**, 2562 (1998).
[37] B. Croonenborghs, F. M. Almeida, S. Cottenier, M. Rots, A. Vantomme, and J. Meersschaut, Appl. Phys. Lett. **85**, 200 (2004).